Special Issue: Vesuvius monitoring and knowledge

The recent seismicity of Mt. Vesuvius: inference on seismogenic processes

Luca D'Auria*, Antonietta M. Esposito, Domenico Lo Bascio, Patrizia Ricciolino, Flora Giudicepietro, Marcello Martini, Teresa Caputo, Walter De Cesare, Massimo Orazi, Rosario Peluso, Giovanni Scarpato, Ciro Buonocunto, Marco Capello, Antonio Caputo

Istituto Nazionale di Geofisica e Vulcanologia, Sezione di Napoli, Osservatorio Vesuviano, Naples, Italy

Article history
Received September 3, 2012; accepted March 1, 2013.
Subject classification:
Mt. Vesuvius, Volcano seismology, Statistical seismology, Volcano monitoring.

ABSTRACT

We have analyzed the recent seismicity of Mt. Vesuvius, with particular emphasis on the period 1999-2012. Since 1972 continuous observations with electromagnetic seismometers allowed the compilation of a detailed earthquake catalogue for the station OVO. Furthermore since 1999 another, more complete, catalogue for the station BKE, closer to the crater, is available. The Gutenberg-Richter distribution of magnitudes shows a temporal decrease of the b-value since 1985, with current values close to 1.0. The temporal pattern of the strain release shows a non-stationary behavior with periods of increased release rates (as in 1989-1990, 1995-1996 and 1999-2000). The spatial distribution of the seismicity consists in two main seismogenic volumes, one with hypocenters clustered below the Mt. Vesuvius crater at depths mostly between 1-6 km, and another with hypocenters clustered within the Gran Cono volcanic edifice, with depths above the sea level. We compare the statistical properties of the seismicity occurring within these two volumes and their spatial and temporal patterns. Moreover we analyze the statistical distribution of focal mechanisms for each volume. Our results point to gravity-induced stresses as the source of the shallow seismicity and of a combined effect of crustal heterogeneities, regional stress and hydrothermal dynamics for the deeper seismicity. Finally we discuss possible future developments of the seismic monitoring system in the light of the past and current seismicity.

1. Introduction

Studying the seismicity of Mt. Vesuvius has an immediate application to the monitoring of this high risk volcano [Orsi et al. 2003, De Natale et al. 2006], but has also an intrinsic scientific interest in understanding the seismicity of a quiescent volcano.

Seismic observations at Mt. Vesuvius started in the second half of the 19th century on the behalf of Luigi Palmieri, director of the Osservatorio Vesuviano (from 1855 to 1903). After the last eruption of Mt. Vesuvius in 1944, the seismicity dropped to low rates (less than 50 events/year). In 1964 it was observed a marked increase in the background volcano-tectonic seismicity [Giudicepietro et al. 2010]. Currently, at the reference station OVO (Figure 1), we observe occurrence rates usually higher than 100 events/year with peaks of more than 600 events/year (in 1996 and 1999).

The permanent seismic network of Mt. Vesuvius (Figure 1) consists of 8 short period 1C, 3 short-period 3C and 9 broadband stations [Orazi et al. 2013]. This network is complemented by temporary stations and by a permanent seismic array. It records hundreds of seismic transients every year, both of natural and artificial origin. They are manually detected and classified on the basis of their type [Iannaccone et al. 2001, Esposito et al. 2013]. Earthquakes are manually picked and, if there are enough seismic phases, they are also located. All the hypocentral parameters and their waveforms are stored in a relational database.

2. Time series analysis

Currently two earthquake catalogues are available for Mt. Vesuvius. The first starts in 1972, ends in June 2012, and contains all the events detected by the OVO station (Figure 1). This station operated almost continuously (> 99%) during the whole period. This catalogue consists in more than 10,500 events, with duration magnitudes (M_d) [Vilardo et al. 1996] ranging from −0.4 to 3.6. In Figure 2 we represent the Gutenberg-Richter (GR) distribution for this dataset. The experimental distribution has been analyzed using the sofware ZMAP [Wiemer 2001] and the inferred b-value is 1.66 ± 0.03 while the magnitude completeness (M_c) is 1.9 ± 0.1.

In Figure 3 we represent the temporal distribution of magnitudes, the event occurrence rate, cumulative

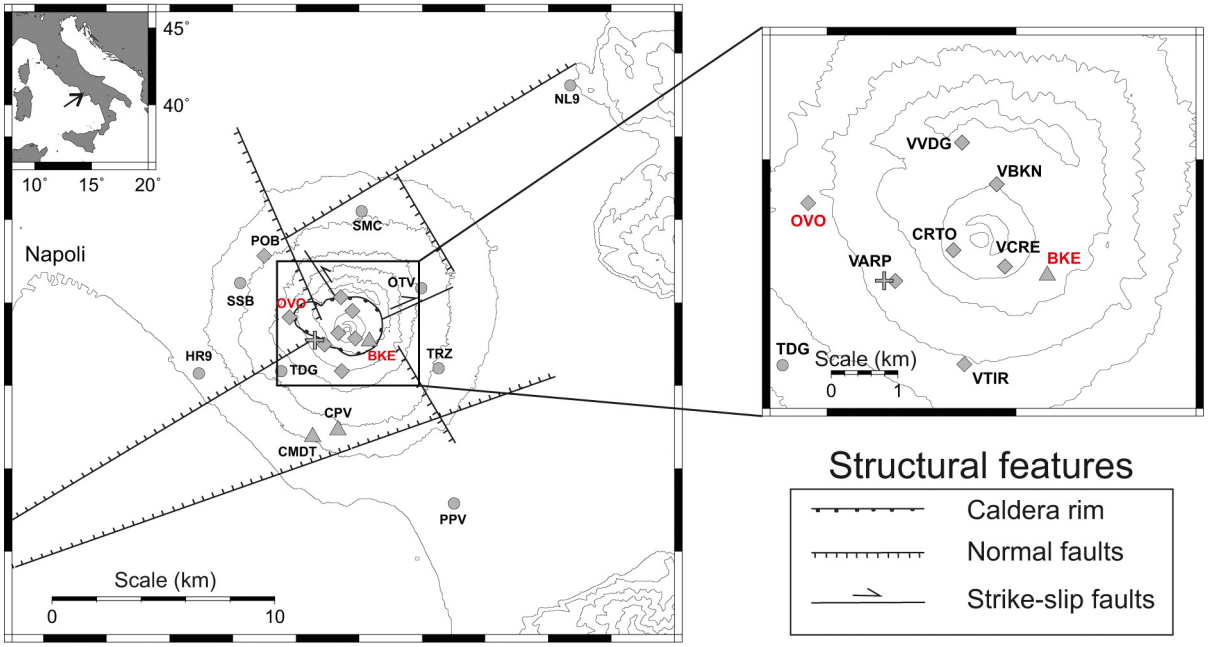

Figure 1. Map of the Vesuvius permanent seismic network. Circles: short-period 1C stations; Triangles: short-period 3C stations; Diamonds, broadband stations. The Vesuvius permanent array is indicated by a cross. Stations BKE and OVO are evidenced in red. Structural features are taken from: Vilardo et al. [1996], Bianco et al. [1998], Orsi et al. [2003].

Benioff strain release [Benioff 1951], the b-value and the M_c. The most striking features are the 4 episodes (marked by the arrows in Figure 3) of increased strain release rate, occurrence rate and event magnitude [Bianco et al. 1999, Capuano et al. 1999, De Natale et al. 2001]. These episodes occurred in 1978-1980, 1989-1990, 1995-1996 and 1999-2000. During the last one, a M=3.6 event was recorded on October 9, 1999. This event, the strongest since the last Mt. Vesuvius eruption in 1944 [Del Pezzo et al. 2004, Giudicepietro et al. 2010], and was widely felt in the Mt. Vesuvius area, reaching a macroseismic intensity of VI MCS at the epicenter [Cubellis and Marturano 2002]. The highest observed occurrence rate is about 700 events/year, in 1999.

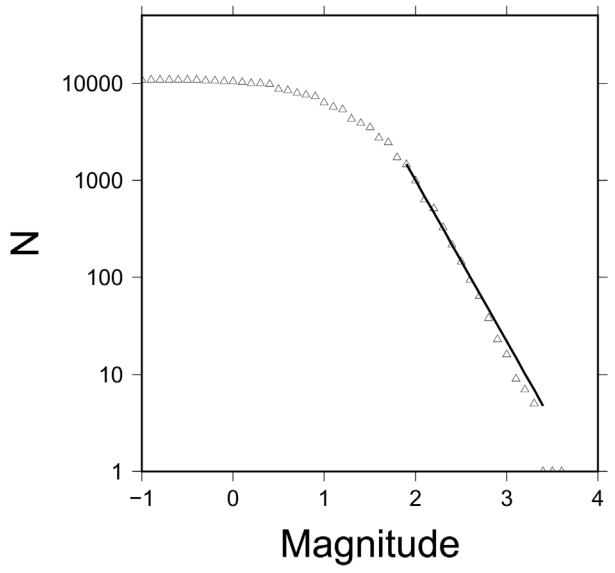

Figure 2. Gutenberg-Richter relationship for the OVO catalogue. The x-axis is the magnitude while the y-axis represents the cumulative number of events. Triangles are the experimental data while the solid line is the theoretical relationship with $a = 6.32$ and $b = 1.66$. The line starts at $M_c = 1.9$.

The temporal variation of the b-value and of M_c has been computed on groups of 100 adjacent events, with an overlap of 25 events. It shows an overall decreasing trend over the whole period, in particular after 1985. This feature was already identified in previous studies [Iannaccone et al. 2001, Zollo et al. 2002b, De Natale et al. 2004]. Here we focus the attention on the period 1999-2012, when the b-value seems to be stable around a value of about 1.1. The temporal variation of M_c shows a general decrease, starting from about 2.0, until 1995 and reaching currently values of about 1.3. This could be related to the transition from analog to digital recording systems [Giudicepietro et al. 2010, Orazi et al. 2013].

The second catalogue contains the events detected by the BKE station (Figure 1). This catalogue starts in 1999, ends in June 2012, and consists in about 10,000 events, with magnitudes ranging from −1.6 to 3.6. As for OVO, BKE station operated almost continuously (> 99%) during this period. Giudicepietro et al. [2010] pointed out by that the differences observed between the OVO and BKE catalogues are related to the peculiar seismicity pattern of Mt. Vesuvius. Since most of the earthquakes occur close to the crater axis, the smallest and shallowest earthquakes are recorded only by the station BKE, which is about 1 km from the crater, while the station OVO is about 2.5 km away.

In Figure 4 we show the GR distribution for the BKE catalogue. The distribution seems to have at least two knees, suggesting that it results from the superposition of two different GR distributions.

We have studied the observed distribution by comparing two alternative models. In the first (A) we hypothesize a simplified model:

$$\log_{10} N(m) = \begin{cases} a^* - b^*(m - M_c) & \text{if } m < M_c \\ a^* - b\ (m - M_c) & \text{if } m \geq M_c \end{cases} \quad (1)$$

where m is the magnitude and $b^* < b$. This distribution is a simplified model of a statistically homogeneous earthquake population. Before the magnitude completeness M_c, the curve has a lower slope b^*, because of the catalogue incompleteness. The actual b-value of the distribution is given by b. The definition of the parameter a^* differs slightly from the commonly used parameter a of the GR distribution: it represents the intercept of the distribution at $m = M_c$. In the second (B) we hypothesize that the observed data are modeled by a a generalization of the standard GR distribution. This distribution consists in the sum of two of the previous model distributions, hence possessing two distinct M_c and b.

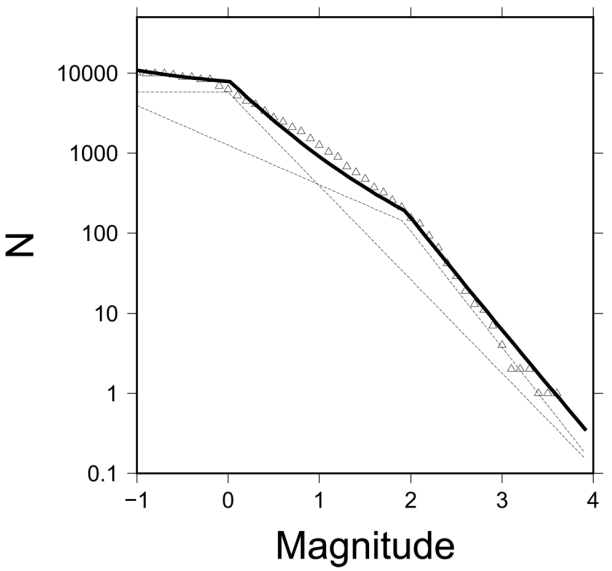

Figure 4. Gutenberg-Richter relationship for the BKE catalogue. Triangles are the experimental data. The dashed lines represent the two theoretical distributions while the solid line is their sum (see Section 2 for details). The b-value of the first distribution is $b = 1.17 \pm 0.06$ while $M_c = 0.0 \pm 0.12$. For the second distribution $b = 1.45 \pm 0.25$ and $M_c = 1{:}91 \_ 0{:}07$.

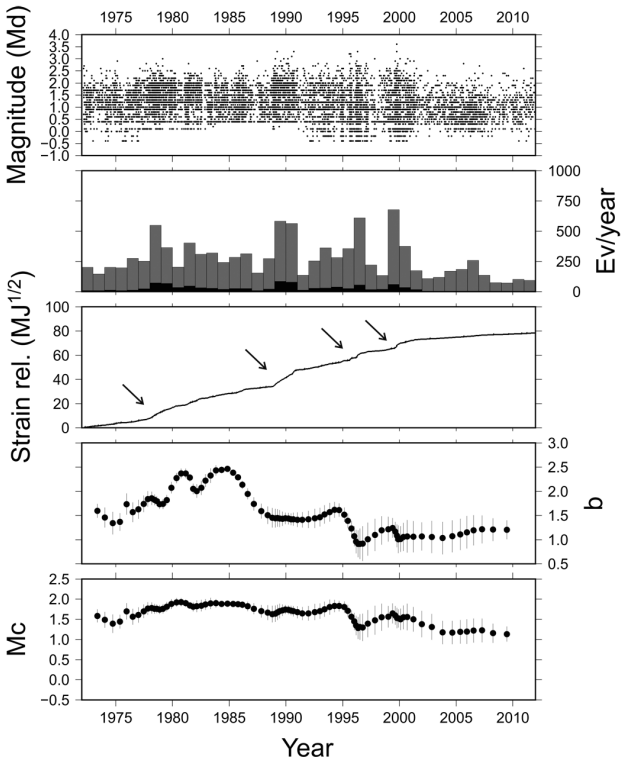

Figure 3. Time series for the OVO catalogue. The first panel shows the event magnitudes while the second one the number of events for each year. The superimposed black histogram represents the number of events having $M \geq 2.0$, which is the maximum value of M_c in the bottom panel. The third represents the cumulative Benioff strain release. Arrows indicate episodes of increased release rate. The fourth panel shows the temporal variation of the b-value. Vertical error bars indicate the 1 σ uncertainty. The last panel shows the M_c values with their 1 σ error bars.

Using a non-linear probabilistic approach, we have fitted the data using these two alternative models. To compare the two models we have used the χ^2 to test the normality of residuals and the Kolmogorov-Smirnov test to check the goodness-of-fit. Results (see Table 1) show that both models provide a reliable fit even if, both tests, show that the double distribution (B) gives a better fit. This is also confirmed by the Akaike Information Criterion (AIC) [Akaike 1974], which provides a helpful means for model selection. AIC values for model B are lower compared to model A (see Table 1). The difference in the AIC values between the two model is 43.88, giving a negligible relative likelihood for model A compared to model B. This strongly supports model B, or in other words that the observed distribution results from the contribution of two distinct fault populations characterized by different statistical properties. In Table 2 we report the best fit values for both models along with their confidence intervals computed using the approach of Jackson and Matsu'ura [1985]. In the model B, the first distribution (B1) has $b = 1.17 \pm 0.06$ and $M_c = 0.0 \pm 0.12$ while the second (B2) has $b = 1.45 \pm 0.25$ and $M_c = 1.91 \pm 0.07$. The higher uncertainty on the determination of the b-value of B2 is caused by the more limited number of data (earthquakes with higher magnitudes) which makes this parameter poorly constrained. In Figure 4 we represent the two theoretical distributions B1 and B2 (dashed lines) and their sum (solid line) compared to the observed overall distribution.

	χ^2 p-value	KS	AIC
A	0.2289	0.351	-65.36
B	0.9477	0.188	-109.24

Table 1. Statistics on the two models tested (A and B). The first colums shows the p-value resulting from a χ^2 test. In both cases it shows that the normality of residuals can be accepted for a statistical significance of at least 5%. The second column shows the ratio between the critical values at a significance level of 5% and the retrieved Kolmogorov-Smirnov statistics. Since both values are lower than 1 the goodness-of-fit is achieved by both models. The third column shows the AIC value for the two models.

	b	b^*	M_c	a^*
A	1.504±0.085	0.51±0.10	1.54±0.06	3.02±0.14
B1	1.17±0.06	0.00±0.21	0.00±0.12	3.72±0.15
B2	1.45±0.25	0.51±0.37	1.91±0.07	2.34±0.12

Table 2. b-value and M_c for the two models. See Section 2 for details.

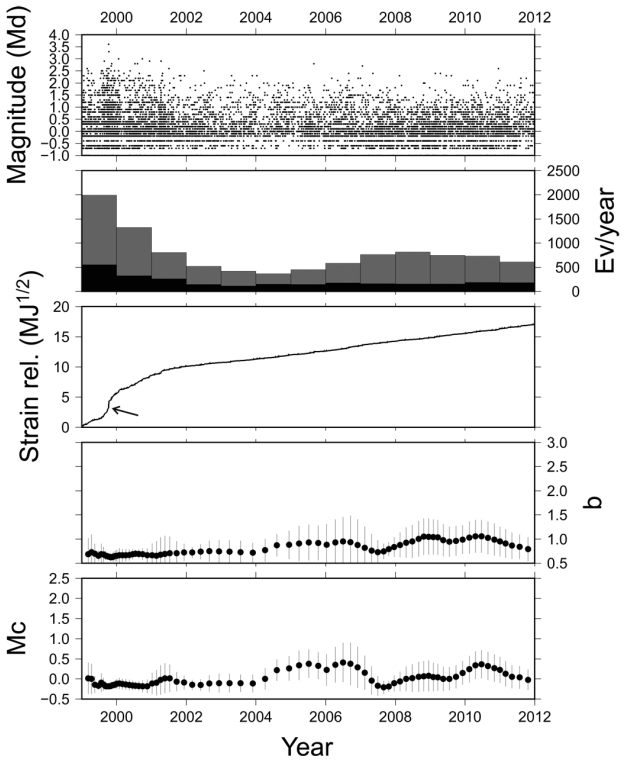

Figure 5. Time series for the BKE catalogue. The meaning of the symbols is the same as for Figure 3. The superimposed black histogram represents the number of events having $M \geq 0.5$, which is the maximum value of M_c in the bottom panel. The arrow indicates the step in the cumulative strain release related to the October 9, 1999, (M=3.6) event.

In Figure 5 we show the temporal distribution of the parameters for the BKE catalogue. The event occurrence rate has a maximum in 1999 with about 2000 events/year. In the following years the rate dropped, reaching a minimum in 2004, with about 400 events/year. In the last 10 years the average occurrence rate at BKE station is about 500 events/year.

The strain release rate (Figure 5) shows a marked increase during the 1999-2000 crisis. Conversely, since 2002 it shows an almost stationary, low rate. As for the OVO catalogue, also the temporal variation of the b-value since 1999, does not show significant trends and is almost stationary with an average value of 0.7. The M_c too, does not show relevant variations.

3. Earthquake locations

We have located the earthquake dataset using a probabilistic approach in a 3D velocity model [Lomax et al. 2001]. The velocity model used in this work consists in a weighted average of three models [D'Auria et al. 2008]. The first model comes from the active seismic experiment TOMOVES96 [Lomax et al. 2001, Zollo et al. 2002a], the second from a local earthquake tomography [Scarpa et al. 2002] and the third from a regional 1D model [Improta et al. 2000]. Details about the merging procedure can be found in D'Auria et al. [2008].

We have relocated events recorded from 1999 to 2000. Among the whole traveltime dataset we were able to locate about 2,400 events having at least 5 phase pickings. All the events belong to the BKE catalogue with about 43% of them belonging also to the OVO catalogue.

Their hypocenters are shown in Figure 6. Most of the epicenters are located within a radius of 3 km from the crater axis. Depths are distributed from about 8 km up to an elevation of 1 km above the sea level (a.s.l.). It is interesting to note that the maximum event depth coincides with the inferred top of the Mt. Vesuvius magma chamber [Auger et al. 2001].

In the two cross-section (Figure 6) it can be seen that earthquakes are grouped in at least two clusters. The first spans mainly the interval between 1 and 5 km depth, while the second is located above the sea level. It should also be noted that earthquakes occurring within the shallow cluster have, generally, lower magnitudes ($M \leq 2.8$) compared to the deeper events.

Hypocentral depths of the deeper cluster are consistent with values determined in previous works regarding the interval 1986-1999. In particular Vilardo et al. [1996], using a dataset of 172 events, showed how during the period 1986-1994 the moment density distribution had two maxima, one at about 4 km depth and another just below the summit of the volcano [see Vilardo et al. 1996, fig. 4c]. Capuano et al. [1999] located about 200 events recorded in the period 1989-1995. They found a concentration of hypocentral depths between 2 and 6 km. Bianco et al. [1999] analyzed the seis-

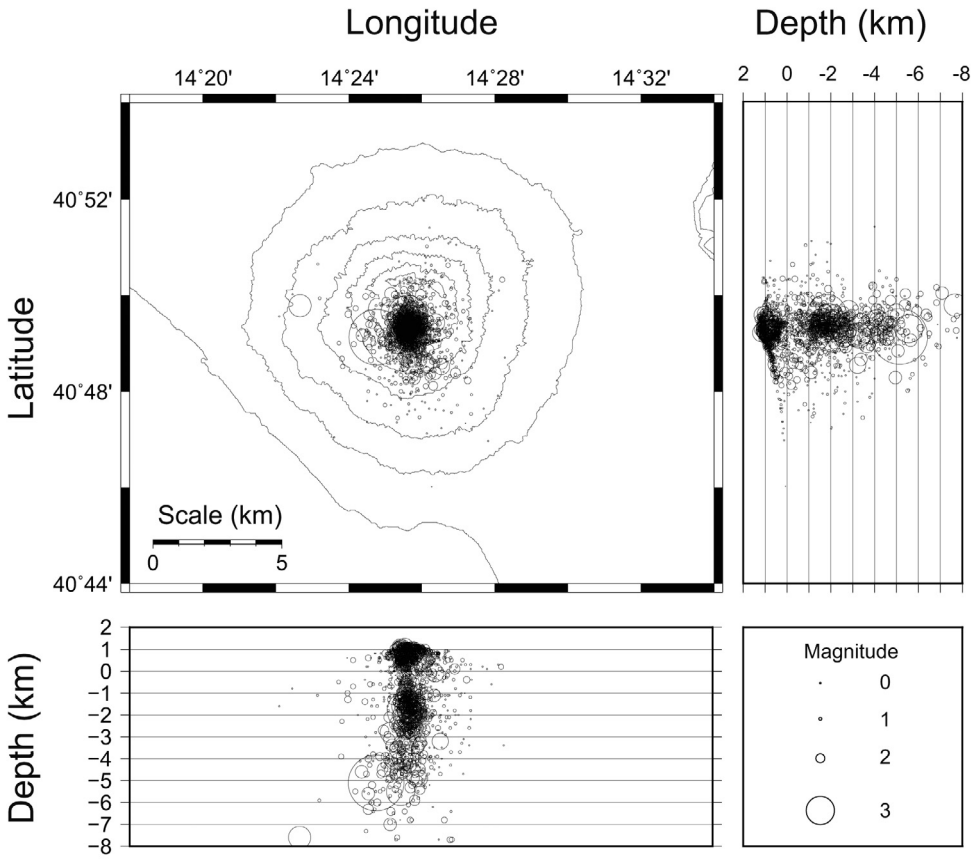

Figure 6. Earthquake hypocenters for the 1999-2012 interval. The top left panel shows earthquake epicenters for events whose location uncertainty (ERH and ERZ) is less than 1 km. The size of simbols is proportional to the event magnitude (see the legend on the lower right). The plot on the left shows hypocenters projected on a NS cross-section, while the lower plot shows an EW cross-section.

micity during two seismic crises occurred at Mt. Vesuvius between August-October 1995 and March-May 1996. They located about 600 events showing that, their hypocentral depths, are distributed mostly between 1 and 4 km. Finally, Zollo et al. [2002b] relocated a dataset of 400 events recorded in the period 1989-1998, showing a concentration of hypocenters between 1 and 5 km depth.

Even if hypocenters occurring within the shallow cluster were already identified by Vilardo et al. [1996] and Bianco et al. [1998], most of the previous papers, dealing with hypocenter location at Mt. Vesuvius, focused mainly on the deep seismicity linked to seismic crises.

4. Strain release

In order to better delineate these two volumes we plot in Figure 7 the spatial distribution of the strain release. Panel A shows the strain release integrated along the vertical direction. It can be seen that most of the strain release occurs within an area of about 1 km^2. In the panel B the strain is integrated along the EW direction, while in panel C along the NS direction. The cross sections clearly delineate the two seismogenic volumes. The first has a peak at a depth of about 2 km and extends between 1 and 7 km. The second has a peak between 0.5 and 1 km a.s.l. The isolated spike indicated by the arrows is relative

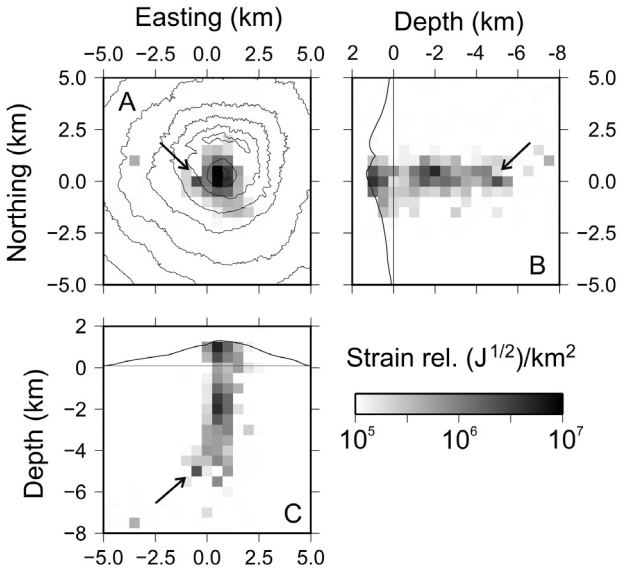

Figure 7. Cumulative strain release. In A we represent the strain release integrated along the vertical direction. In B the integration is performed along the EW direction while in C along the NS direction. The arrows point to a strain release spike related to the October 9, 1999, (M=3.6) event. The grids used in the plots are equally spaced with an interval of 500 m.

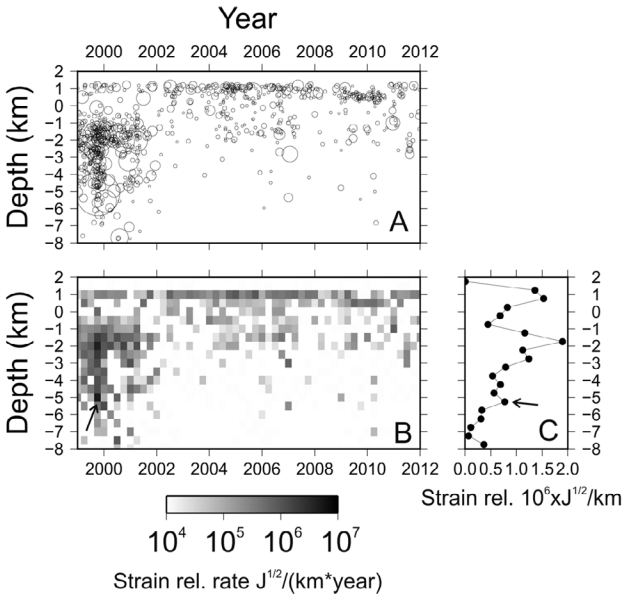

Figure 8. Time-depth distribution of the strain release. In A we plot events in a time-depth graphic. Symbol sizes are proportional to magnitude as for Figure 6. In B we represent the strain release as a function of time and depth. In C we show the strain release as a function of the depth. The arrows in B and C point to the strain release spike related to the October 9, 1999, (M=3.6) event.

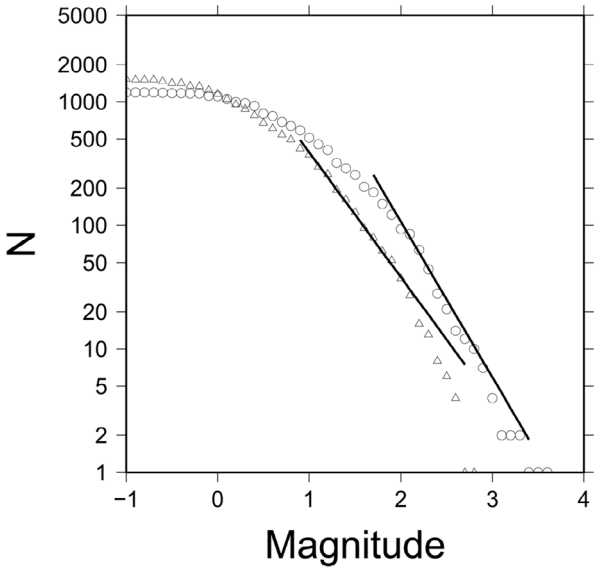

Figure 9. Gutenberg-Richter relationship for located earthquakes. Triangles are experimental data for events located a.s.l. while circles are for the deeper events. The theoretical relationship for triangles has parameters $b = 1.01$ and $a = 3.6$ with $M_c = 0.9$. For the circles the parameters are $b = 1.26$, $a = 4.55$ and $M_c = 1.7$.

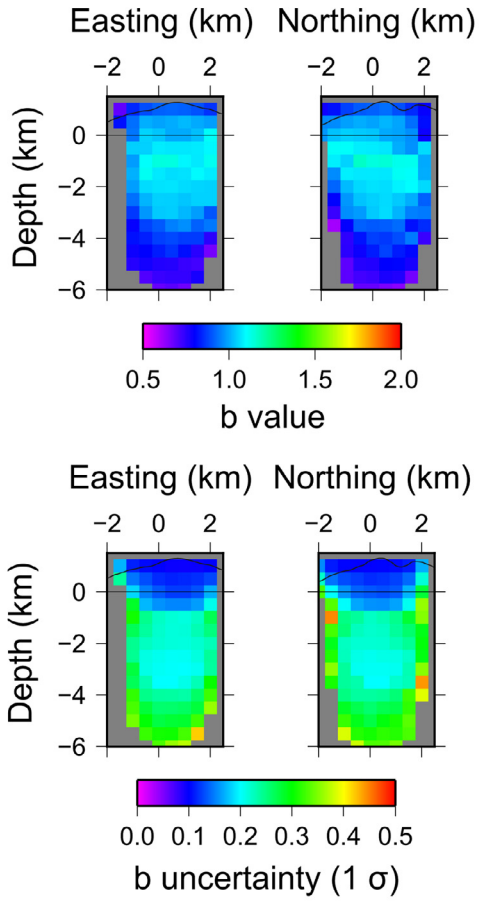

Figure 10. Spatial distribution of the b-value. The two panels on the top represent the b-value distribution along an EW (left) and a NS (right) cross-section. The two cross-sections intersect on the Mt. Vesuvius crater. The bottom panels represent the uncertainty on the retrieved b-values.

to the October 9, 1999, (M=3.6) event, located at about 5.6 km depth.

We have already analyzed, in Figures 3 and 5, the temporal variation of the strain release rate. In Figure 8 we represent the strain release as a function of both time and depth. In panel B it can be seen that, until 2002, the strain was released mostly by the deeper volume while, since then, most of the strain has been released within the shallow volume. Panel C shows the strain release as a function of depth. This graphic shows unambiguously that a zone of very reduced strain release occurs between the shallow and the deep seismogenic volumes. The separation between the two volumes is located at a depth of about 1.0 km.

Moreover, the curve of panel C, has a clear asymmetry in the part below 1 km depth. It increases sharply and then slowly decays with depth.

5. B-value analysis

To characterize the seismogenic processes occurring within the two volumes we have studied the spatial distribution of the b-value. In Figure 9 we plot the GR distribution for events located since 1999, separately for the shallow cluster (triangles) and for the deep one (circles). The b-value for the shallow cluster is 1.01 ± 0.05, while for the deep is 1.26 ± 0.08. The respective M_c are 0.9 ± 0.15 and 1.7 ± 0.1. The GR distribution for the BKE catalogue (Figure 4), discussed in Section 2 can now be justified in terms of a superposition of two distributions related to two different seismogenic volumes. The shallow volume seems to correspond to the first

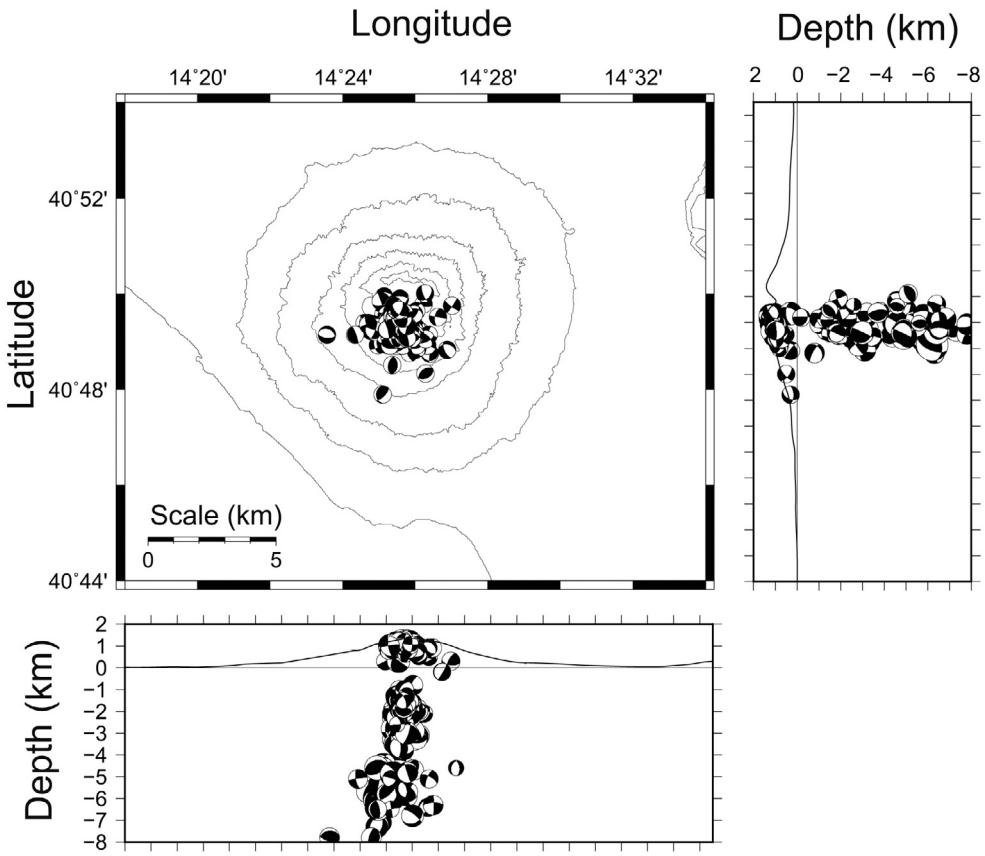

Figure 11. Focal mechanisms for 195 events. Beach-balls are projected on the horizontal plane (top left), on a NS cross-section (top right) and on a EW cross-section (bottom).

distribution (having $b = 1.17 \pm 0.06$ and $M_c = 0.0 \pm 0.12$) while the deep volume to the second distribution (with $b = 1.45 \pm 0.25$ and $M_c = 1.91 \pm 0.07$).

A more clear understanding of the spatial distribution of the b-value can be seen in Figure 10. This figure shows the b-value along two orthogonal cross sections (EW and NS) intersecting on the Mt. Vesuvius crater. For each point we have computed the b-value and its uncertainty, using all the events located within a radius of 2 km from the point itself. Points are regularly spaced on a 3D grid with a spacing of 0.5 km. Only volumes containing at least 30 events have been used. The uncertainty in the b-value estimate increases for depths higher than 3 km because of the decreasing earthquake spatial density (Figure 10).

Both the EW and the NS cross sections show similar patterns. Above the sea level the b-value varies between 0.7 and 1. It increases with depth, showing a maximum value of about 1.5, at 1 km depth. Below this depth, it decreases steadily, reaching a value of about 0.6 at 6 km depth. It should be noted that the b-value estimates are poorly reliable below 4 km (Figure 10).

The spatial distribution of the b-value seems to indicate a difference in the seismogenic processes between the two volumes and a variation within the deep volume itself. In particular this analysis confirms that the shallow volume is characterized, on average, by a lower b-value compared to the deeper volume. Furthermore the correct determination of the spatial distribution of the b-value is fundamental in seismic risk studies [Convertito and Zollo 2011].

6. Focal mechanisms

We have computed focal mechanisms for events having at least 8 P-wave polarities. This subset consists in 197 events, with magnitudes ranging from 1.8 to 3.6. Focal mechanisms have been computed using the FPFIT software [Reasenberg and Oppenheimer 1985].

In Figure 11 we show the mechanisms projected on the horizontal plane and along two NS and EW cross-sections. They do not seem to have a clear preferential orientation, neither a predominant fault type. This can be seen more clearly in Figures 12 and 13. The first figure shows the fault type classified on the basis of the rake angle (Aki and Richards [2002] convention). The panel A is for events located a.s.l. It shows a dominance of strike and reverse mechanisms. In panel B the histogram refers to events located below the sea level. In this case the mechanisms are almost equally distributed among all the fault types.

In Figure 13 we represent also the azimutal distribution of fault strike angles, separately for shallow and deep events. Shallow events show a marked predominance of WNW direction, while for deep events

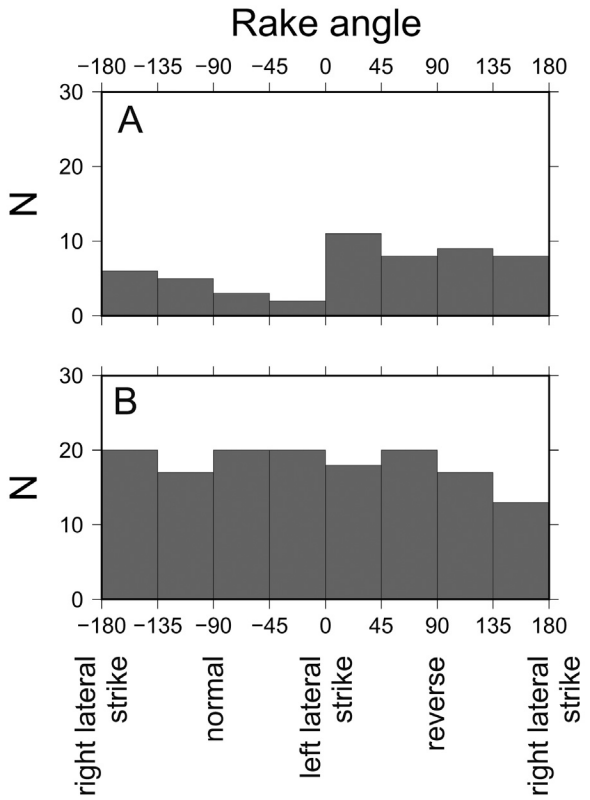

Figure 12. Distribution of rake angles for the mechanisms of Figure 11. In A we represents rake angles of events located a.s.l. while in B the same for the other events.

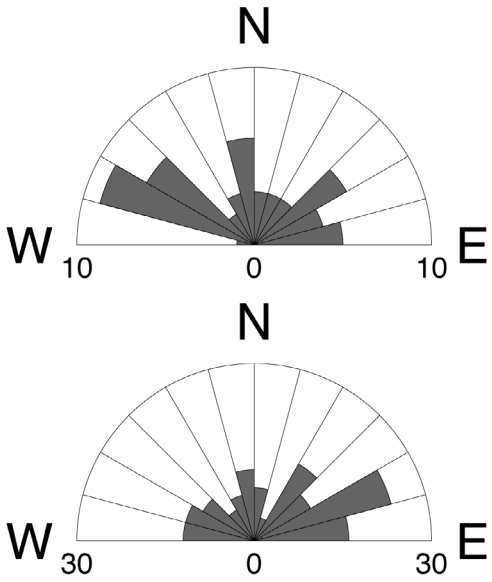

Figure 13. Rose diagram showing the distribution of strike values of the focal mechanisms. The graphic on the top is for events located a.s.l. while the one on the bottom is for the other events. Each sector is 15° wide and the outer edge of the graphics corresponds to a value of 10 events for the top and 30 for the bottom.

the preferential direction is ENE. Both directions are compatible with the faulting pattern observed at regional and local scales (see structural features delineated in Figure 1) [Vilardo et al. 1996, Bianco et al. 1998, Orsi et al. 2003].

To better understand the relationship between the faulting pattern and the stress field we plot in Figure 14 the tension, the neutral and the pressure axes of the focal mechanisms for shallow and deep events. In both cases the pattern is quite scattered. For deep events there seems to be a concentration of P axes in the SE sector of the graphic. This direction is compatible with the regional stress field retrieved from GPS measurements and borehole breakout data [Barba et al. 2010, Pierdominici et al. 2011].

7. Discussion

The results presented in the previous sections highlight at least 3 important features of the recent seismicity at Mt. Vesuvius.

The first is the presence of two main seismogenic volumes: one located between 1 and 7 km, and another between 0.5 and 1 km a.s.l. The strain release of the deep volume occurs mostly between 1 and 3 km (Figure 8).

The second is that the deep volume is characterized, on average, by a higher b-value compared to the shallow one (1.26 *versus* 1.01) (Figure 9). However it should be noticed that the b-value varies with depth within this volume, ranging from 1.5 at 1 km depth to 0.6 at 6 km depth. This trend is similar to the strain release pattern (Figure 8) which, for the deep volume, starts at 1 km depth, reaches a maximum at 2 km depth and then decreases, becoming almost null at 7 km depth. The similar patterns suggest the existence of a relationship between these two parameters and their link with the seismogenic processes. A similar pattern was also evidenced by Del Pezzo et al. [2004], which showed how the stress drop of shallow earthquakes (< 2.6 km) is lower (around 1 bar), while for deeper earthquakes (> 4 km) is higher (10 bar), reaching a maximum value of about 100 bar for the October 9, 1999, (M=3.6) event.

The third observation is that the focal mechanism distribution is different within the two volumes. In the shallow volume it does not show a dominant orientation of P and T axes. This, together with the almost stationary strain release within this volume (see Section 4), suggests that the contribution of gravitational stresses may be an important factor for the seismogenesis within this volume. Actually, the concentration of shear stresses along the slopes of a relief, has been assessed using both analytical and numerical approaches [Martel and Muller 2000]. Furthermore, the the low values of the lithostatic load, existing at shallow depth, favours the occurence of shear failure [Russo et al. 1997]. In this case the orientation of P and T axes would

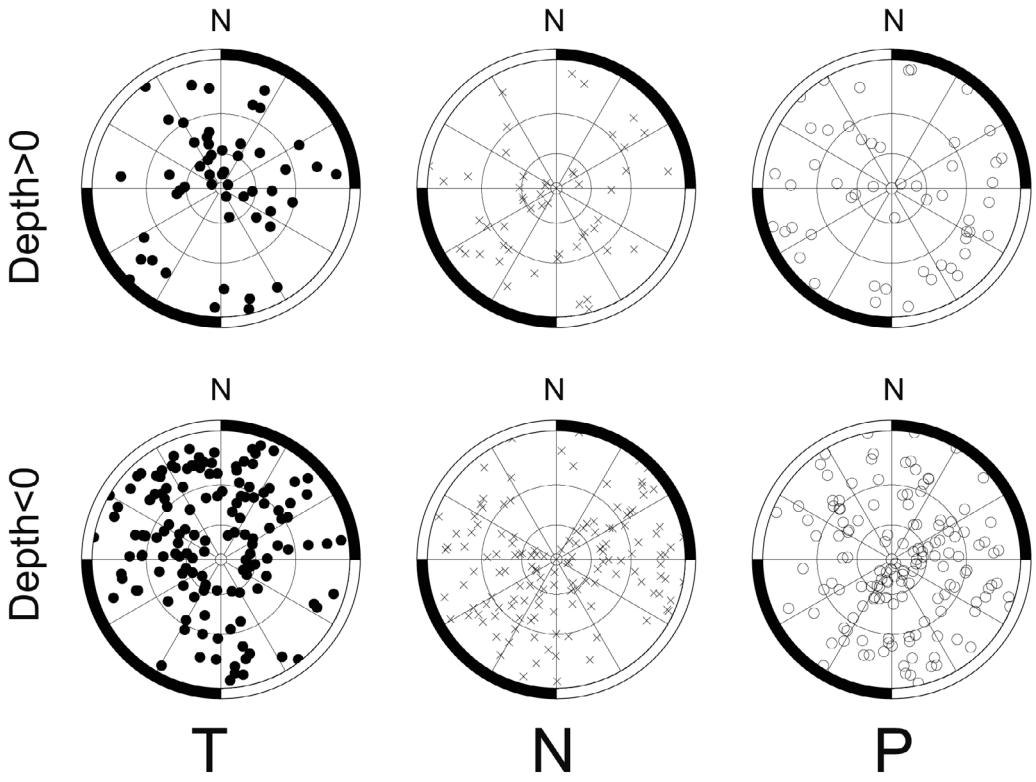

Figure 14. Stereographic plots of tension (T), neutral (N) and pressure (P) axes for the focal mechanisms of Figure 11. The graphics on the top represent data for events located a.s.l. while those on the bottom are for the other events.

be strongly dependent on the topography, hence justifying the absence of a clear dominant orientation. To support this hypothesis we also notice that the measurement of ground deformation at Mt. Vesuvius have shown a long term trend of downward and radially outward motion [Lanari et al. 2002]. This pattern has been interpreted as the result of a slow spreading of the volcanic edifice under the effect of the gravitational loading [Borgia et al. 2005]. The clayey ductile layer identified by Borgia et al. [2005] and responsible of the spreading roughly concides with the level of reduced strain release, separating the two seismogenic volumes. This suggests that it could be also related to observed volume of reduced strain release existing between 0.5 km a.s.l. and 1 km depth (Figure 8).

Concerning the deep volume, various hypothesis about the seismogenic mechanism have been proposed. Bianco et al. [1998] suggested a dominant role of the regional stress field, while De Natale et al. [1998] proposed that a local crustal heterogeneity (in particular a central high rigidity body) plays a significant role in the seismogenesis. The analysis of focal mechanisms, indicates that both mechanisms could act simultaneously. The P axes distribution (Figure 14) shows a prevalence in the SE sector, even if with a significant scattering. This seems to suggest that, focal mechanism at Mt. Vesuvius, result from the superposition of a regional stress field and local perturbations induced by the complexity of the volcanic structures.

However, these two factors are not able to justify the observed temporal patterns in the strain release (Figures 3 and 5) and in the time-depth-strain relationship (Figure 8). On other active volcanoes, like Campi Flegrei (see D'Auria et al. [2011], and references therein), a causal link has been established between episodes of magmatic fluid injection in the hydrothermal system, and an increase in the seismicity.

A connection between the Mt. Vesuvius hydrothermal system and seismogenesis has been already recognized by Madonia et al. [2008] and Caliro et al. [2011]. In particular, the latter work, points to a deep magmatic origin of fluids perturbing the shallow hydrothermal system, which feeds the Mt. Vesuvius crater fumaroles. They also recognized significant variations accompanying the 1999-2000 seismic crisis. In their model the hydrothermal systems host a high-temperature ($T = 450°$) reservoir of NaCl rich brines, at depth approximately between 2.5 and 5 km. The position of the top of this reservoir is consistent with the area of highest strain release. The higher b-values found at these depths (Figure 10) are consistent with the presence of high pore pressure. In other volcanic system high b-values have been interpreted as a possible evidence of proximity to a magma chamber [Power et al. 1998, Wiemer et al. 1998]. However, at Mt. Vesuvius, there is no evidence of shallow magma chambers [Zollo et al. 2002a]: a possible magma layer has been

recognized only at about 8 km depth [Auger et al. 2001].

From a seismological point of view, indirect evidences of the role of fluids is given by the analysis of short-term statistical properties of the seismicity. At a global scale the seismicity of Mt. Vesuvius has statistical features similar to tectonic earthquakes [Bottiglieri et al. 2009]. However, Godano et al. [1997] and Zollo et al. [2002b], using different approaches, have shown that at a smaller time scale the seismicity of Mt. Vesuvius is clustered, showing a dominant tendency of earthquakes to occurr within seismic swarms. This is a common feature of the seismicity observed in volcanic areas [Zollo et al. 2002b] and in general the occurrence of seismic swarms can often be explained in terms of pore pressure driven processes [Yamashita 1999].

Another indirect evidence of the role of fluids was given by Pandolfi et al. [2006] which, using coda-wave interferometry, detected velocity variations preceeding and following the 1999-2000 crisis. They interpreted that variation as the effect of a fluid pressure increase before the crisis and its subsequent drop.

All these evidences point to a tight link between the dynamics of the hydrothermal system and the spatio-temporal pattern of the seismicity. Concerning the temporal decrease in the b-value between 1985 and 1999, Zollo et al. [2002b] proposed that it could be related to a decrease in the pore pressure. They observed that the b-value decrease has been accompanied by a progressive decrease in the temperature of Mt. Vesuvius fumaroles.

The increase of the seismicity, observed in 1978-1980, 1989-1990, 1995-1996 and 1999-2000, could be explained as the results of the injection of fluid batches, of magmatic origin, at the bottom of the hydrothermal system. The upward migration of these fluids can be the cause of the pore pressure increase and consequently of the seismicity. A similar mechanism has been observed in the recent dynamics of Campi Flegrei caldera [D'Auria et al. 2011].

The vertical variation of the thermodynamical properties of the hydrothermal system could also explain the observed variations of the strain release, the stress drop and the b-value with depth. It may be justified by a decrease of the pore pressure with depth in parallel with the increase of the lithostatic load.

8. Conclusions

The study of the Mt. Vesuvius seismicity, since 1999, allowed to identify two separate seismogenic volumes. The first, shallower, is located above the sea level, within the Mt. Vesuvius volcanic edifice. This seismicity is characterized by low magnitudes and by a low b-value (about 1.01). The temporal distribution of the strain release is quite stationary (Figure 8) compared to the events located within the deeper volume which seem to occurr preferentially during seismic crises [Vilardo et al. 1996, Bianco et al. 1999, Capuano et al. 1999, De Natale et al. 2004]. We postulate that the seismicity within this volume is mostly driven by shear stressed induced by the gravity.

The second, deeper, seismogenic volume, extends from about 1 up to 7 km depth. The characteristics of its seismicity point to heterogeneous stress field, resulting from the superposition of a regional field and (strong) local perturbations induced by density and rigidity variations at kilometric scales, occurring below the volcanic edifice. This stress field alone is not able, usually, to be a causative source of seismicity. With the support of direct (geochemical) and indirect (seismological) evidences, we postulate that, fluids within the hydrothermal system of Mt. Vesuvius, play a fundamental role in modulating the occurrence of earthquakes within this volume. The temporal modulation of the seismicity, or in other words, the occurrence of seismic crises at Mt. Vesuvius, is likely to be caused by the injection of fluids, from the magma chamber (at about 8 km depth) [Auger et al. 2001], within the Mt. Vesuvius hydrothermal system. After the 1999-2000 crisis, until 2012, the seismicity of Mt. Vesuvius has been characterized by a stationary pattern, consisting mainly in the occurrence of low-magnitude earthquakes within the shallow volume.

Accurate 3D numerical modeling of the stress field together with a thermo-fluid-dynamical modeling of the hydrothermal system, could shed light on some still unresolved questions. The most important are the nature of the reduced strain release volume existing between 0.5 km a.s.l. and 1 km depth and the origin of the vertical variations in the seismicity patter observed below 1 km depth.

Our results also give some hints concerning future improvements of the seismic monitoring system. The difference between the M_c for the whole BKE catalogue and that for the located events indicates the necessity of further lowering the capability to locate small ($M < 0$) earthquakes. Efforts in this direction have been already carried out, putting more stations close the epicentral area (Gran Cono), achieving a significative drop in the M_c for events located at shallow depth [Orazi et al. 2013]. A further improvement can be achieved by enhancing the signal/noise ratio. Currently, a reliable approach to this problem, is to replace surface stations with borehole installations. Another possibility is to complement, standard location procedures, with seismic array analysis.

Lastly, since the temporal and spatial variations of

the b-value have shown to be important parameters: they should be included in the seismic monitoring system as routine analyses.

Acknowledgements. We are grateful to Bruno Massa for the useful discussion about the determination of the stress field and Ada De Matteo for revising the focal mechanisms dataset. We are also grateful to two anonymous reviewers, whose valuable suggestions and constructive criticisms, improved the manuscript.

References

Akaike, H. (1974). A new look at the statistical model identification, IEEE Trans. on Automatic Control, 19 (6), 716-723.

Aki, K., and P.G. Richards (2002). Quantitative Seismology, University Science Books.

Auger, E., P. Gasparini, J. Virieux and A. Zollo (2001). Seismic evidence of an extended magmatic sill under Mt. Vesuvius, Science, 294, 1510-1512.

Barba, S., M.M.C. Carafa, M.T. Mariucci, P. Montone and S. Pierdominici (2010). Present day stress field modelling of Southern Italy constrained by stress and GPS data, Tectonophysics, 482, 193-204; doi: 10.1016/j.tecto.2009.10.017.

Benioff, H. (1951). Earthquakes and rock creep. (part I: creep characteristics of rocks and the origin of aftershocks), Bull. Seismol. Soc. Am., 41 (1), 31-62.

Bianco, F., M. Castellano, G. Milano, G. Ventura and G. Vilardo (1998). The Somma-Vesuvius stress field induced by regional tectonics: evidences from seismological and mesostructural data, J. Volcanol. Geoth. Res., 82, 119-218.

Bianco, F., M. Castellano, G. Milano, G. Vilardo, F. Ferrucci and S. Gresta (1999). The seismic crises at Mt. Vesuvius during 1995 and 1996, Phys. Chem. Earth (A), 24 (11-12), 977-983.

Borgia, A., P. Tizzani, G. Solaro, M. Manzo, F. Casu, G. Luongo, A. Pepe, P. Berardino, G. Fornaro, E. Sansosti, G.P. Ricciardi, N. Fusi, G. Di Donna and R. Lanari (2005). Volcanic spreading of Vesuvius, a new paradigm for interpreting its volcanic activity, Geophys. Res. Lett., 32, L03303; doi:10.1029/2004GL022155.

Bottiglieri, M., C. Godano and L. D'Auria (2009). Distribution of volcanic earthquake recurrence intervals, J. Geophys. Res., 114, B10309; doi:10.1029/2008JB005942.

Caliro, S., G. Chiodini, R. Avino, C. Minopoli and B. Bocchino (2011). Long time-series of chemical and isotopic compositions of Vesuvius fumaroles: evidence for deep and shallow processes, Annals of Geophysics, 54 (2), 137-149; doi:10.4401/ag-5034.

Capuano, P., U. Coppa, G. De Natale, F. Di Sena, C. Godano and C. Troise (1999). A detailed analysis of some local earthquakes at Somma Vesuvius, Annali di Geofisica, 42 (3), 391-405.

Convertito, V., and A. Zollo (2011). Assessment of precrisis and syn-crisis seismic hazard at Campi Flegrei and Mt. Vesuvius volcanoes, Campania, southern Italy, Bull. Volcanol., 73, 767-783; doi:10.1007/s00445-011-0455-2.

Cubellis, E., and A. Marturano (2002). Mt. Vesuvius: a macroseismic study of the earthquake of 9 October 1999, J. Volcanol. Geoth. Res., 118, 339-351.

D'Auria, L., M. Martini, A. Esposito, P. Ricciolino and F. Giudicepietro (2008). A unified 3D velocity model for the neapolitan volcanic areas, In: W. Marzocchi and A. Zollo (eds.), Conception, verificatio and application of innovative techniques to study active volcanoes, INGV-DPC, 375-390. ISBN:978-88-89972-90-0.

D'Auria, L., F. Giudicepietro, I. Aquino, G. Borriello, C. Del Gaudio, D. Lo Bascio, M. Martini, G.P. Ricciardi, P. Ricciolino and C. Ricco (2011). Repeated fluid-transfer episodes as a mechanism for the recent dynamics of Campi Flegrei caldera (1989-2010), J. Geophys. Res., 116, B04313; doi:10.1029/2010JB007837.

Del Pezzo, E., F. Bianco and G. Saccorotti (2004). Seismic source dynamics at Vesuvius volcano, Italy, J. Volcanol. Geoth. Res., 133, 23-29.

De Natale, G., P. Capuano, C. Troise and A. Zollo (1998). Seismicity at Somma-Vesuvius and its implications for the 3D tomography of the volcano, J. Volcanol. Geoth. Res., 82, 175-197.

De Natale, G., C. Troise, F. Pingue, P. De Gori and C. Chiarabba (2001). Structure and dynamics of the Somma-Vesuvius volcanic complex, Mineralogy and Petrology, 73, 5-22.

De Natale, G., I. Kuznetov, T. Kronrod, A. Peresan, A. Sarao, C. Troise and G.F. Panza (2004). Three decades of seismic activity at Mt. Vesuvius: 1972-2000, Pure Appl. Geophys., 161, 123-144.

De Natale, G., C. Troise, F. Pingue, G. Mastrolorenzo and L. Pappalardo (2006). The Somma-Vesuvius volcano (Southern Italy): structure, dynamics and hazard evolution, Earth-Science Reviews, 74, 73-111.

Esposito, A.M., L. D'Auria, F. Giudicepietro, T. Caputo and M. Martini (2013). Neural analysis of seismic data: applications to the monitoring of Mt. Vesuvius, Annals of Geophysics, 56 (4), S0446; doi:10.4401/ag-6452.

Giudicepietro, F., M. Orazi, G. Scarpato, R. Peluso, L. D'Auria, P. Ricciolino, D. Lo Bascio, A.M. Esposito, G. Borriello, M. Capello, A. Caputo, C. Buonocunto, W. De Cesare, G. Vilardo and M. Martini (2010). Seismological monitoring of Mount Vesuvius (Italy): More than a century of observations, Seismol. Res. Lett., 81 (4), 625-634; doi:10.1785/gssrl.81.4.625.

Godano, C., M.L. Alonzo and G. Vilardo (1997). Multifractal approach to time clustering of earthquakes: application to Mt. Vesuvius seismicity, Pure Appl. Geophys., 149, 375-390.

Iannaccone, G., G. Alessio, G. Borriello, P. Cusano, S. Petrosino, P. Ricciolino, G. Talarico and V. Torello (2001). Characteristics of the seismicity of Vesuvius and Campi Flegrei during the year 2000, Annali di Geofisica, 44 (5-6), 1075-1091.

Improta, L., G. Iannaccone, P. Capuano, A. Zollo and P. Scandone (2000). Inferences on the upper crustal structure of Southern apennines (Italy) from seismic refraction investigations and subsurface data, Tectonophysics, 317 (3-4), 273-298.

Jackson, D.D., and M. Matsu'ura (1985). A bayesian approach to nonlinear inversion, J. Geophys. Res., 90 (B1), 581-591.

Lanari, R., G. De Natale, P. Berardino, E. Sansosti, G.P. Ricciardi, S. Borgstrom, P. Capuano, F. Pingue and C. Troise (2002). Evidence for a peculiar style of ground deformation inferred at Vesuvius volcano, Geophys. Res. Lett., 29 (9), 1292; doi:10.1029/2001 GL014571.

Lomax, A., A. Zollo, P. Capuano and J. Virieux (2001). Precise, absolute earthquake location under Somma-Vesuvius volcano using a new three-dimensional velocity model, Geophys. J. Int., 146, 313-331.

Madonia, P., C. Federico, P. Cusano, S. Petrosino, A. Aiuppa and S. Gurrieri (2008). Crustal dynamics of Mount Vesuvius from 1998 to 2005: Effects on seismicity and fluid circulation, J. Geophys. Res., 113, B05206; doi:10.1029/2007JB005210.

Martel, S.J., and J.R. Muller (2000). A two-dimensional boundary element method for calculating elastic gravitational stresses in slopes, Pure Appl. Geophys., 157, 989-1007.

Orazi, M., L. D'Auria, A. Tramelli, C. Buonocunto, M. Capello, A. Caputo, W. De Cesare, F. Giudicepietro, M. Martini, R. Peluso and G. Scarpato (2013). The seismic monitoring network of Mt. Vesuvius, Annals of Geophysics, 56 (4), S0450; doi:10.4401/ag-6456.

Orsi, G., S. de Vita, M.A. Di Vito, R. Isaia, R. Naveand and G. Heiken (2003). Facing volcanic and related hazards in the Neapolitan area, In: R. Fakundiny, G. Heiken and J. Sutter (eds.), Earth Science in a City: A Reader, AGU, 127-170. ISBN:0-87590-299-5.

Pandolfi, D., C.J. Bean and G. Saccorotti (2006). Coda wave interferometric detection of seismic velocity changes associated with the 1999 M=3.6 event at Mt. Vesuvius, Geophys. Res. Lett., 33, L06306; doi: 10.1029/2005GL025355.

Pierdominici, S., M.T. Mariucci and P. Montone (2011). A study to constrain the geometry of an active fault in southern Italy through borehole breakouts and downhole logs, J. Geodyn., 52, 279-289.

Power, J.A., M. Wyss and J.L. Latchman (1998). Spatial variations in the frequency magnitude distribution of earthquakes at Soufriere Hills volcano, Montserrat, West Indies, Geophys. Res. Lett., 25 (19), 3653; doi:10.1029/98GL00430.

Reasenberg, P.A., and D. Oppenheimer (1985). Fpfit, fpplot and fppage: Fortran computer programs for calculating and displaying earthquake fault plane solutions, USGS Technical Report 85-739.

Russo, G., G. Giberti and G. Sartoris (1997). Numerical modeling of surface deformation and mechanical stability of Vesuvius volcano, Italy, J. Geophys. Res., 102 (B11), 24785-24800.

Scarpa, R., F. Tronca, F. Bianco and E. Del Pezzo (2002). High resolution velocity structure beneath Mount Vesuvius from seismic array data, Geophys. Res. Lett., 29, 2040; doi:10.1029/2002GL015576.

Vilardo, G., G. De Natale, G. Milano and U. Coppa (1996). The seismicity of Mt. Vesuvius. Tectonophysics, 261, 127-138.

Wiemer, S., S.R. McNutt and M. Wyss (1998). Temporal and three-dimensional spatial analyses of the frequency–magnitude distribution near Long Valley caldera, California, Geophys. J. Int., 134 (2), 409-421; doi:10.1046/j.1365-246x.1998.00561.x.

Wiemer, S. (2001). A software package to analyze seismicity: ZMAP, Seismol. Res. Lett., 72, 373-382.

Yamashita, T. (1999). Pore creation due to fault slip in a fluid-permeated fault zone and its effect on seismicity: Generation mechanism of earthquake swarm, Pure Appl. Geophys., 155 (2-4), 625-647; doi: 10.1007/s000240050280.

Zollo, A., L. D'Auria, R. De Matteis, A. Herrrero, J. Virieux and P. Gasparini (2002a). Bayesian estimation of 2-D P-velocity models from active seismic arrival time data: imaging of the shallow structure of Mt. Vesuvius (Southern Italy), Geophys. J. Int., 151, 566-582.

Zollo, A., W. Marzocchi, P. Capuano, A. Lomax and G. Iannaccone (2002b). Space and time behavious of seismic activity and Mt. Vesuvius volcano, Southern Italy, Bull. Seismol. Soc. Am., 92 (2), 625-640.

*Corresponding author: Luca D'Auria,
Istituto Nazionale di Geofisica e Vulcanologia, Sezione di Napoli, Osservatorio Vesuviano, Naples, Italy;
email: luca.dauria@ov.ingv.it.